Engineering of electrospun polyimide separators for electrical double-layer capacitors and lithium-ion cells

Jui-Yu Pai[1,2], Cheng-Ta Hsieh[1], Chih-Hung Lee[1,3], Jeng-An Wang[1], Hao-Yu Ku[1],

Chun-Lung Huang[1], Laurence J. Hardwick[2,*] Chi-Chang Hu[1,*]

[1]*Laboratory of Electrochemistry and Advanced Materials, Department of Chemical Engineering, National Tsing Hua University, Hsinchu 30013, Taiwan*

[2]*Stephenson Institute for Renewable Energy, Department of Chemistry, University of Liverpool, Liverpool L69 3BX, United Kingdom*

[3]*Materials and Chemical Research Laboratories, Industrial Technology Research Institute, Hsinchu 30013, Taiwan*

Abstract

Functionalised polyimide (PI) separators, with high electrolyte wettability and good thermo-dimensional stability, in combination with electrolytes provide ionic conductivities > 1 mS for electrical double-layer capacitors (EDLCs) and lithium-ion batteries (LIBs). The mechanical strength of PI separators can be further improved by a factor of 3 via the optimisation of ratio of soft and hard segments, and the introduction of 5% SiO_2 nanoparticles (NPs). The electrolyte uptake capability and ionic conductivity of this copolymerized PI separator is also promoted by the addition of SiO_2 NPs, favouring the high-rate performances of EDLCs and LIBs. The cyclic voltammetry (CV) curves of an EDLC with this separator show the rectangle shape of a typical capacitor, indicating the low ionic resistance of this copolymerised PI separator. For the usage in the LIBs, on the other hand, a coating of low-density polyethylene (LDPE) onto this PI-SiO_2 (PI-SiO_2@PE) separator enables the thermal shutdown function of a LIB without sacrificing cell performance. There is no significant change in morphology for this PI-SiO_2@PE separator after the 50-cycle full cell test, indicating its promising application potential in LIBs. The study has demonstrated the ability to tailor the multi functionality of the polyimide separator to optimise it properties for specific applications.

Keywords: separator, polyimide, electrical double-layer capacitor, lithium-ion battery.

1. Introduction

For energy storage devices (e.g., lithium-ion batteries (LIBs) and supercapacitors (SCs)), the separators prevents electronic contact between positive and negative electrodes but permits ionic flow from the incorporated liquid electrolyte. [1, 2]. Low ionic resistance of separators is an essential factor for reduction in joule heating and enhancement of energy efficiency. In particular, this is important for high-power devices (e.g., SCs and power-type LIBs) to satisfy both present and future demands for the high-rate charge-discharge performance [3, 4].

Separators in most energy storage devices should provide various functions in order to meet safety and performance requirements [5-7]. For instance, strong mechanical strength is one of the vital characteristics to keep the spiral wound structure of LIBs and electrical double-layer capacitors (EDLCs) from damages during fabrication [8]. In addition, separators should be able to prevent the physical contact between positive and negative electrodes under both normal and high temperature environments, [6, 7, 9] since the internal temperature of cells will become much higher during the charge-discharge cycling. Temperature gradients within cells will be further exacerbated at high current densities [7, 10, 11]. Consequently, the thermo-dimensional stability (i.e. the ability of the separator to maintain its shape over a range of temperatures) is considered to be an important factor determining the reliability and safety of high-power devices.

Apart from the above basic requirements, the safety issue is always the first priority in considering lithium-based energy storage devices (LIBs, Li-ion capacitors (LICs), and metallic Li batteries (LBs)) [7]. When cells overheating, such as the occasional for example via short-circuits [7, 12], thermal runaway may occur, which generally results from the decomposition of solid electrolyte interphase (SEI) layer, followed by melting of separator, and then irreversible ignition of explosion fuel by the solvent in the electrolyte and O_2 release from the positive electrode. Consequently, the thermal shutdown function, i.e., thermal closure of pores within the separator to interrupt the ionic flow between two electrodes [13], is an additional necessary requirement of separators. Moreover, demands for the high C-rate charge-discharge capability of batteries [14-17] and SCs [18-21] become more and more popular. Hence, porosity and ceramic NPs modifications in separators are usually employed to improve the performance of LIBs/LBs and SCs in recent years [7] although most reports focused on improving one or two properties of the separators for LIBs or SCs [1, 22-24].

Nowadays, the most common separators used in LIBs are porous polyolefin films consisting of polyethylene (PE), polypropylene (PP), or their tandem sandwich structure [9] meanwhile the commercially available separators utilised within EDLCs are composed of cellulose [4]. Polyolefin separators generally have excellent mechanical strength, good chemical stability, and reasonable cost. However, one of the serious issues

within LIB applications for PE-based separators is the severe shrinkage at relatively elevated temperatures, increasing the risk of internal short circuit from direct contact between positive and negative electrodes. [1, 8, 9, 12] The sandwich-type PP/PE/PP separator circumvents the thermal shrinkage issue, because the high melting point PP servers as the mechanical support for the low melting point PE that works as the pore blocking agent. However, the risk of short circuit risk remains when the cell temperatures are equal to/above 140^{o}C [25]. In addition, the electrolyte wettability of polyolefin separators is poor, because of their non-polar characteristics elevating the ionic resistance and directly affecting the battery performance [9, 13, 26, 27]. Accordingly, the required functions of separators vary strongly depending on their applications. As a consequence, separator design that optimises key characteristics, such as mechanical strength, chemical stability, electrolyte wettability and permits high ionic conductivity, as well as the purpose-oriented functions like the thermal shutdown function for lithium-based batteries and dendrite inhibition for lithium metal batteries, is key development.

Herein electrospun PI-based separators with controllable thickness are reported [13, 28, 29] to possess the typical separator functions of high mechanical strength, good chemical stability, excellent electrolyte wettability, and low ionic resistance, applicable to both EDLCs and high-voltage SCs [30]. The optimisation of the soft and hard segment ratio in the copolymerised PI with the addition of 5% SiO_2 NPs significantly promotes

the mechanical strength of resultant separators. The electrolyte uptake capability and ionic conductivity of this copolymerized PI separator is also promoted by the addition of SiO_2 NPs, favouring the high-rate performances of EDLCs and LIBs. Moreover, the purpose-oriented function of thermal shutdown for the LIB and LIC applications can be added onto the separator via a simple spin-coating process.

2. Experimental

2.1. Materials

Pyromellitic dianhydride (PMDA), phenylenediamine (PDA), and 4,4-oxydianiline (ODA) were commercial products from Echo Chemical Co. (Taiwan). Silicon (IV) oxide NPs from Alfa Aesar, Thermo Fisher Scientific Co. (USA). Polyvinylpyrrolidone (PVP, Mw = 1300000), dimethylformamide (DMF), and p-xylene were purchased from Sigma Aldrich Co. (USA). The low-density polyethylene (LDPE) was from USI Co. (Taiwan). Celgard 2325 membrane with a thickness of 25 μm (Celgard USA) was used as the separator of LIBs for a comparison purpose. TF4030 separator (thickness of 30 μm, Nippon Kodoshi Co., Japan) was used as the reference separator applied to EDLCs. The electrolyte used for LIBs was commercially available from Ubiq Tech. Co. (Taiwan) 1 M $LiPF_6$ in a mixed carbonated solution (ethyl methyl carbonate/diethyl carbonate/ethylene carbonate, EMC/DMC/EC =1/1/1 with 1% vinylene carbonate, VC). The electrolyte for

EDLCs was a solution of 1 M tetraethylammonium tetrafluoroborate/propylene carbonate ($TEABF_4$/PC), both salt and solvent were purchased from Sigma Aldrich Co. (USA). The ionic conductivities of both electrolytes were 10.5 $mS \cdot cm^{-1}$ and 13 $mS \cdot cm^{-1}$. All reactants were analytical grade and used as received without any further purification.

2.2.Preparation of co-polymerised PI nanofibre (Co-PI), silica-co-electrospun Co-PI (Co-PI-SiO_2), LDPE-coated Co-PI (Co-PI@PE), and LDPE-coated Co-PI-SiO_2 (Co-PI-SiO_2@PE)

Copolymerised polyamic acid (Co-PAA) solutions were prepared from the mixtures with various ratios of ODA and PDA (O/P = 7/3, 6/4, 5/5, 4/6 and 3/7), which reacted with an equivalent molar ratio of PMDA in DMF at room temperature. Then, 20 wt.% PVP was added into the PAA solution to improve the spinability (the ability to reshape polymers into a fibre). 5 wt.% SiO_2 NPs were added into the above precursor solution to prepare the Co-PAA solution containing SiO_2 NP (Co-PAA-SiO_2). The above polymer solutions were loaded onto a syringe at a flow rate of 0.3-0.5 mL h^{-1} under a voltage of 24-27 kV during the electrospinning process [31, 32]. Co-PAA and Co-PAA-SiO_2 fabrics were heated in an oven at 300°C for 2 h to obtain the Co-PI and Co-PI-SiO_2 nanofabrics [32]. For polyimide, its PAA precursor solution was synthesised by the polymerisation of ODA and PMDA, and was electrospun to form the PAA fabrics which were converted to polyimide by heating at 300^oC for 2 h. These fabrics were shaped into circles with 16 mm

in diameter for the EDLC application. For the usage in LIBs, a spin-coating procedure was applied to prepare a thin LDPE layer onto the above separators according to the steps proposed previously [26] to obtain the Co-PI@PE and Co-PI-SiO_2@PE separators.

2.3. Separator Characterisation

The surface morphologies and fibre diameters of various separators were examined by scanning electron microscopy (SEM, Hitachi S-4200) and transmission electron microscopy (TEM, JEOL JEM-F200). The pore size distribution was measured by a capillary flow porometer (PMI Inc.). The porosity of separators was quantified by soaking in the n-butanol using the following Equation [27]:

$$\mathrm{P}(\%) = \frac{\frac{M_{BuOH}}{\rho_{BuOH}}}{\frac{M_{BuOH}}{\rho_{BuOH}}+\frac{M_P}{\rho_P}} \times 100\% \qquad (1)$$

where M_p is the mass of a dry separator and M_{BuOH} is the mass of the corresponding separator soaked with n-butanol for 2 h. The electrolyte uptake was measured by a similar method and n-butanol was substituted by the electrolytes used for EDLCs or LIBs [33]:

$$\text{Electrolyte uptake} = \frac{W_1 - W_0}{W_0} \times 100\% \qquad (2)$$

where W_0 is the dry separator and W_1 is the soaked one. The 1 M $TEABF_4$/PC and 1 M $LiPF_6$/(EC/DMC/EMC) with 1 % VC electrolytes were used to examine the static contact angle by means of a commercial drop shape system (First Ten Angstrom Co.). Thermogravimetric analysis (TGA, TA Q600, USA) was conducted from room

temperature to 700°C at a heating rate of 10°C min^{-1} under an airflow. Thermal-dimensional stability of separators was examined in an oven at 110, 130 and 150°C for 1 h. The mechanical strength was measured by a universal testing machine (HT8160 Hung Ta Instrument Co., Taiwan) clamping both sides of the films with a shape of 5×2 cm at a stretching rate of 50 mm min^{-1}.

The conductivity of separators was measured by the electrochemical impedance spectroscopic (EIS) method under the open-circuit state with an alternating current (AC) amplitude of 10 mV from 1 to 100 kHz in a Swagelok cell with two stainless steel (304) in the diameter of 15.8 mm as electrodes via an electrochemical system (CHI600, CHI instrument, USA). The conductivity of soaked separators was estimated from the bulk resistance (R_b) obtained at the high-frequency end through Equation (3) [34]:

$$\sigma = \frac{d}{R_b \times A} \qquad (3)$$

where σ (mS·cm^{-1}), d (cm), and A (cm^2) are ionic conductivity, thickness of separators, and area of separators, respectively. The Li/electrolyte interfacial resistance was measured in a similar way while the electrodes were replaced with two lithium metal electrodes. The potential window of separators determined by linear sweep voltammetry (LSV) was conducted in a Swagelok cell where lithium metal and stainless steel (304) electrodes were the reference and counter electrodes, respectively.

The full cell tests for both EDLCs and LIBs were conducted by assembling electrodes,

separators, and electrolyte to a coin-type cell (CR2032). The volumes of electrolytes added into all coin cells was fixed to be 100 μL. Karl Fisher titration KF Coulometer (Metrohm Ag. Co., Switzerland) determined the water content in the electrolyte to be below 5 ppm. The full cells of LIBs with the positive $LiFePO_4$ and negative mesocarbon microbead electrodes ($LiFePO_4$//MCMB, capacity = 138 mAh g^{-1}) were examined by a battery testing equipment (Land CT2001A, China). All the electrodes materials were ready-to-use commercial products coated onto current collectors (provided by Ubiq Tech. Co., Taiwan). The mass loadings of $LiFePO_4$ and MCMB were 17.5 mg cm^{-2} and 6 mg cm^{-2}, respectively. The rate test of LIBs was conducted from 0.1 to 2 C and the cycling test was examined under 0.5 C for 50 cycles. The charge-discharge voltage window was between 2.5 and 4.2 V. After the charge-discharge cycling tests, the separators were taken out, rinsed with carbonate solvent for the morphology examination by SEM.

In EDLCs, activated carbon-coated Al electrodes were prepared by a doctor-blade coating method (activated carbon, ACS25, CPC. Co., Taiwan). The mass loading on both electrodes was 1 mg cm^{-2}. The cyclic voltammograms (CVs) were measured between 0 and 2.5 V. The galvanostatic charge-discharge test was conducted within the same voltage window at various current densities.

3. Results and Discussion

3.1.Basic function comparisons of separators

The microstructure of Co-PAA is composed of microblocks including the rigid segment of PDA and the soft segment of ODA. These microblocks were thermally transformed into Co-PI resulting in the uniform distribution within the PI nanofibres. This structure was found to reduce the local stress accumulation and avoid the fibre breaking [35]. Accordingly, the mechanical strength of PI-based separators can be improved by the copolymerisation with a suitable ratio of the hard and soft segments.

Table 1 shows the physicochemical properties of Co-PI separators prepared from the precursor solutions in various ODA/PDA (O/P) ratios. The mechanical strength is shown to increase with decreasing the ODA/PDA (O/P) ratio. When the O/P ratio is equal to 5/5, the mechanical strength of this Co-PI separator (denoted as Co-PI-5/5) reaches the maximum of 12.5 MPa. The data highlights that Co-PI with the suitable ratio of the flexible and rigid microblocks enables the stress to pass throughout the whole fabric. The porosity of polyimide and Co-PI is lowered by decreasing the ODA/PDA (O/P) ratio. Since the porosity of the same series separators should affect the uptake number of electrolytes, the ionic conductivity of Co-PI-5/5 should be slightly lower than that of polyimide (see below).

Table 1. Physicochemical properties of Co-PI separators prepared from the precursor solutions in various ODA/PDA (O/P) ratios.

Property \ O/P ratio	**7/3**	**6/4**	**5/5**	**4/6**	**3/7**	**Polyimide**
Stress (MPa)	6.5	8.8	12.5	7.4	5.8	5.7
Porosity (%)	88	85	82	79	77	92

The stress-strain curves of Co-PI-5/5 (co-polymer of polyimide transformed from the Co-PAA with the ODA/PDA ratio of 5/5), polyimide, Co-PI-5/5-SiO_2 and polyimide-SiO_2 separators are illustrated in Figure 1. The Co-PI-5/5-SiO_2 and polyimide-SiO_2 separators were transformed from the Co-PAA and PAA fabrics with 5 wt% SiO_2 nanoparticles (SiO_2 NPs) added in the electrospinning precursor solutions. Overall, all the mechanical strength of the separators synthesised by co-polymerisation is much higher than the baseline polyimide. The stretch ratio of polyimide was found to be over 130%, and is much greater than Co-PI-5/5 (about 100%). In addition, the mechanical strength of both separators is promoted by the introduction of SiO_2 NPs since the mechanical strength increases by 23% to approximately 16 MPa and 72% to around 10 MPa for Co-PI-5/5 and polyimide separators, respectively. This phenomenon is attributable to that SiO_2 NPs are utilised as a filler which has been entangled uniformly in the nanofibre during the electrospinning process. Consequently, the composite

nanofibres can convey the stress to SiO_2, further supporting the stress to keep from the local excess load happening.

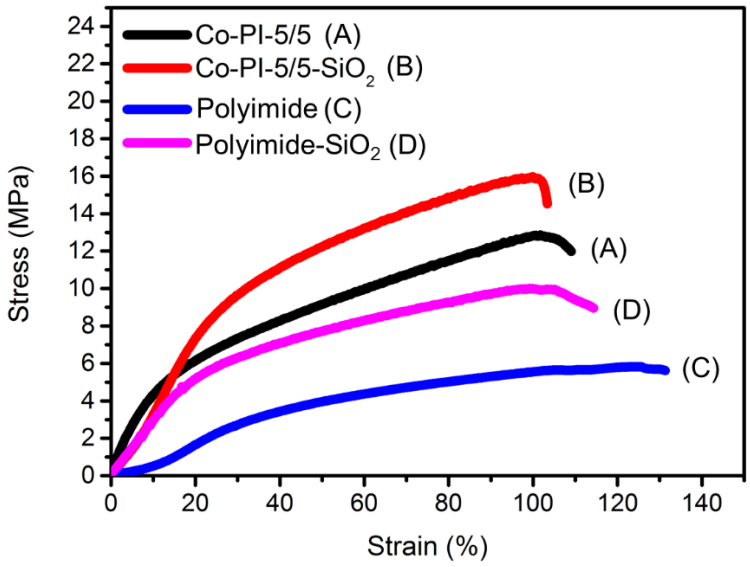

Figure 1. The stress-strain curves of (A) Co-PI-5/5, (B) Co-PI-5/5-SiO_2, (C) polyimide, and (D) polyimide-SiO_2 separators; 5 wt% SiO_2 NPs were added in the electrospinning Co-PAA or PAA solutions for preparing the composite separators.

Table 2 demonstrates the influence of introducing SiO_2 NPs on the physicochemical properties of Co-PI-5/5 and compares the important properties of the Co-PI-5/5-SiO_2 separator with a commercially available separator, TF4030, for the EDLC application. Note that the porosity of Co-PI-5/5-SiO_2 is slightly higher than Co-PI-5/5 while its electrolyte uptake capacity is significantly enhanced. The former result is probably due to a larger internal electrostatic repulsion force of Co-PI-5/5-SiO_2, which makes thinner fibres in comparison with Co-PI-5/5 (see Figures S1 and S2 in the Supporting

Information). The latter result indicates the enhanced electrolyte affinity of Co-PI through the introduction of SiO_2 NPs.

Table 2. Physicochemical properties of polyimide, Co-PI-5/5 and Co-PI-5/5-SiO_2 and TF4030, a commercial EDLC separator.

Electrolyte	A (LIBs)			B (SCs)		
Types of separator	Polyimide	Co-PI-5/5	Co-PI-5/5-SiO_2	Co-PI-5/5	Co-PI-5/5-SiO_2	TF4030
Thickness (μm)	25	25	25	30	30	30
Porosity (%)	92	82	84	85	87	54
Electrolyte uptake (%)	1550	1360	1420	1250	1370	165
Ionic conductivity (mS cm^{-1})	1.68	1.19	2.13	0.88	1.16	0.79
MacMullin number	6.3	8.8	4.9	14.8	11.2	16.5

Remark: The electrolytes used for A (LIBs) and B (SCs) are 1 M $LiPF_6$ in a mixed carbonate solution (EC/DMC/EMC = 1/1/1 with 1 % VC) and 1 M $TEABF_4$/PC, respectively.

For the LIB application, the ionic conductivity of this Co-PI-5/5-SiO_2 separator (2.13 mS cm^{-1}) with its electrolyte uptake capacity of 1420% is greater than those of Co-PI-5/5 and polyimide separators (1.19 and 1.68 mS cm^{-1}) with the electrolyte uptake capacity of 1360% and 1550%, respectively. Accordingly, the ionic conductivity within the separator is affected by not only porosity and electrolyte uptake capability, but also the interactions among functional groups (e.g., Si-OH) on the separators, solvent molecules, and ions.

For the SC application, Table 2 illustrates that the electrolyte uptake ability and ionic conductivity of Co-PI-5/5-SiO_2 are higher than those of TF4030 which has been utilized in the commercial EDLCs. Interestingly, this result matches the results of the contact

angle test shown in the Supporting Information (Figure S3), reasonably due to that the electrolyte wettability of Co-PI-5/5 is a little higher than that of TF4030, which is much lower than that of Co-PI-5/5-SiO_2. Moreover, the results of ionic conductivity (Figure S4) also increase by about 0.28 mS cm^{-1} after the addition of SiO_2 NPs in the fibre, revealing that the ceramic materials with a good affinity to electrolytes show the ability to enhance the ionic conductivity. Since the ionic conductivity of Co-PI-5/5-SiO_2 is higher than that of Co-PI-5/5, the Co-PI-5/5-SiO_2 separator will show better charge-discharge performance than Co-PI-5/5 when the current density becomes higher.

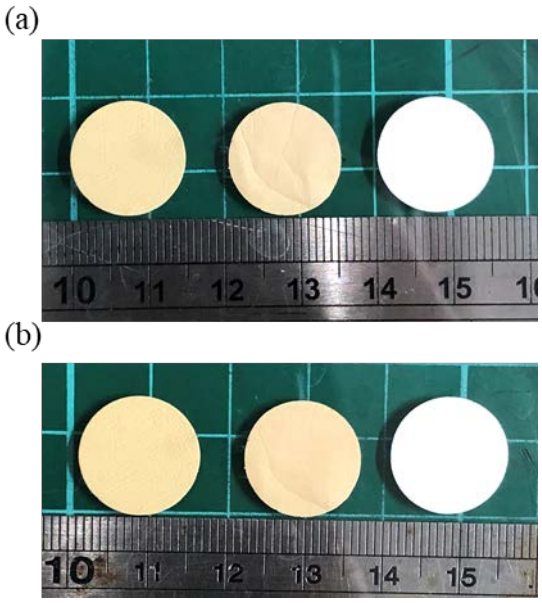

Figure 2. Photographs s of (left) Co-PI-55, (middle) Co-PI-5/5-SiO_2, and (right) TF4030 separators (a) before and (b) after heating at 150°C for 1 h.

The thermo-dimensional stability of Co-PI-55, Co-PI-5/5-SiO_2, and TF4030

separators was tested in an oven at 150^{o}C for 1 h. The results are shown in Figure 2. All these films do not undergo dimension shrinkage after the thermal test, revealing their excellent thermo-dimensional stability. It is reasonable because both PI fabrics were derived from PAA annealed at 300^{o}C for 2 h. In fact, the thermo-dimensional stability of separators applied to SCs must be no shrinkage before the temperature above 150^{o}C because the high-power characteristics of such devices will increase the internal temperature during the repeated high-rate charge-discharge cycling.

3.2. Separators for the SC application.

The capacitive performances, included CVs, galvanostatic charge-discharge curves, and Nyquist plots, of symmetric AC-coated EDLCs assembled with various separators are displayed in Figure 3. In Figure 3a, the CV curves of all cells recorded at 10 mV s^{-1} between 0 and 2.5 V are overlapped each other and exhibit a rectangular shape without any redox peaks. These results demonstrate the typical capacitor behaviour of these EDLCs with very rapid charge-discharge responses. Accordingly, Co-PI-5/5 and Co-PI-5/5-SiO_2 show the promising application potential as the commercial separator in the EDLC application.

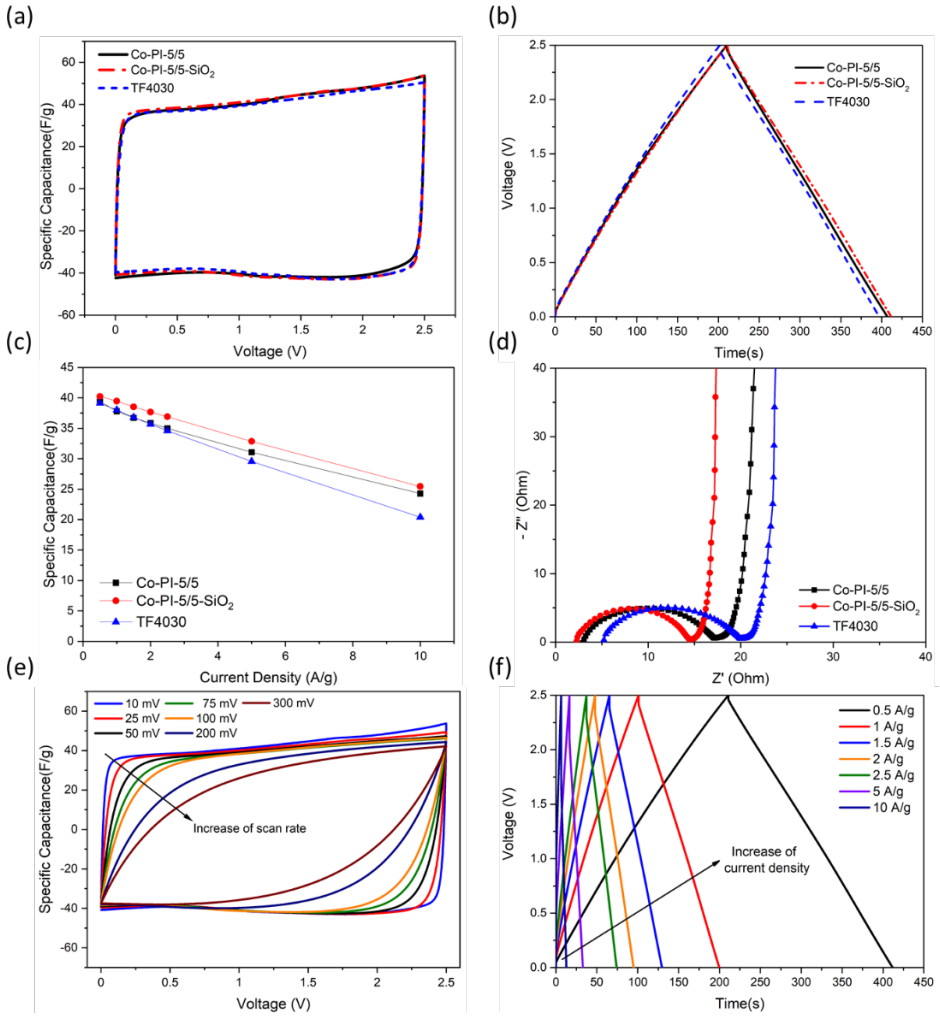

Figure 3. (a) CVs, (b) galvanostatic charge-discharge curves, (c) specific capacitance-current density curves, and (d) Nyquist plots of the EDLC with (1) Co-PI-5/5, (2) Co-PI-5/5-SiO_2, and (3) TF4030 separators. (e) CVs at various scan rates and (f) galvanostatic charge-discharge curves at various current densities of the EDLC using the Co-PI-5/5-SiO_2 separator.

Figure 3b represents the typical galvanostatic charge-discharge curves of the above three EDLCs measured at 0.5 A g^{-1}. The data show no discernible difference in the cell

capacitance of these three cells measured at a relatively low current density; consequently, most of the active materials can be utilised. However, when the current density is gradually increased (see Figure 3c and Figure S5 in the Supporting Information), the difference in the cell capacitance becomes distinguishable because the iR effect increases with the applied current density. As a result, a little higher resistance can be found in the cell using the TF4030 separator. This effect leads to the variation in the capacitance retention for the cells using the Co-PI-5/5, Co-PI-5/5-SiO_2, and TF4030 separators equal to 61.7, 63.3 and 52.1%, respectively when the current density rises from 0.5 to 10 A g^{-1}.

The above phenomena can be further examined by the electrochemical impedance spectroscopic (EIS) analysis. The EIS data are presented as the Nyquist plots in Figure 3d. From these EIS spectra, all cells show near identical responses and the vertical responses in the low-frequency region reveal the typical EDLC behaviour, indicating that Co-PI-5/5 and Co-PI-5/5-SiO_2 are promising separators in the EDLC application. Note in the high- and middle-frequency regions of these EIS spectra that two impedance elements can be found, i.e., the equivalent series resistance (ESR) obtained at the high-frequency end (which mainly depends on electrolyte conductivity, thickness and material of the separator) and the charge-transport impedance, Z_{CT} (which can be separated into two components: the electronic and ionic resistances [36] and both components rely on the electrode). The electronic resistance includes the intrinsic electronic conductivity of AC

particles, the electronic contact between particles, and the interfacial contact between the active layer and current collector. The ionic component generally depends on the thickness of the active layer, the active layer/electrolyte interface, as well as the electrolyte conductivity inside the pores and porous texture of electrodes [37-40]. From Figure 3d, the order of separators with respect to increasing the cell ESR is: Co-PI-5/5-SiO_2 (2.2 Ω) < Co-PI-5/5 (3.0 Ω) < TF4030 (5.1 Ω). According to Equation (3), the ionic conductivity of these separators can be obtained from the cell ESR. Clearly, the Co-PI-5/5-SiO_2 separator exhibits the highest ionic conductivity of 0.77 mS cm^{-1}, which is much higher than TF4030 with an ionic conductivity of 0.33 mS cm^{-1}. The above results reveal that Co-PI-5/5-SiO_2 shows a good ability to conduct ions, resulting in the highest cell capacitance retention at high current densities. The real part resistance of Z_{CT} can be estimated from the diameter of the semicircle in the EIS spectra, which is slightly reduced by the introduction of SiO_2 NPs into the Co-PI-5/5 separator, probably due to the improvement at the active layer/electrolyte interface since the resistances of the two cells using Co-PI-5/5 and TF4030 are similar.

The CV curves of the coin cell employing Co-PI-5/5-SiO_2 measured at various scan rates are also displayed in Figure 3e. The CVs maintain the rectangular-like shape up to 100 mV s^{-1} (charge or discharge time is ca. 25 seconds), reflecting the rapid ion transport and fast charge-discharge responses [41]. The galvanostatic charge-discharge results

measured at various current densities in Figure 3f strongly support the above statement because all of the galvanostatic charge-discharge curves exhibit symmetric triangular profile [42]. From all the above results and discussion, the Co-PI-5/5-SiO_2 film is a promising candidate for the separator of EDLCs because all its physicochemical properties meet the application requirement of EDLCs with a spirally wound assembly.

3.3. Separators for the LIB application.

For the application of separators in LIBs, the thermal shutdown functionality can be added via the spin coating of a thin LDPE layer onto the Co-PI-5/5 and Co-PI-5/5-SiO_2 separators. The surface morphologies and cross-section images of Co-PI-5/5@PE and Co-PI-5/5-SiO_2@PE separators are examined in Figure 4. In Figure 4a, a uniform and thin layer of LDPE has been coated onto this Co-PI-5/5 film, which does not block the pore within the film because of the absence of obvious aggregations. Figure 4b also shows a uniform coating of LDPE on the Co-PI-5/5-SiO_2@PE separator. The SiO_2 NPs uniformly dispersed on the fibres in the Co-PI-5/5-SiO_2@PE film are clearly visible in Figure 4c, indicating that the introduction of SiO_2 NPs does not affect the uniformity of this thin LDPE layer conducted by the spin coating method. From Figures 4d and 4e, the cross-section images of Co-PI-5/5@PE and Co-PI-5/5-SiO_2@PE display that the LDPE layer has been incorporated into the upper layer of the separator. Consequently, there is no significant difference in overall thickness and properties between the LDPE-coated

separators and their original counterparts except for the thermal shutdown function added on the former separators. The above statement is supported by the results of the contact angle test showing the high electrolyte affinity of these LDPE-coated separators (see Figure S6 in the Supporting Information).

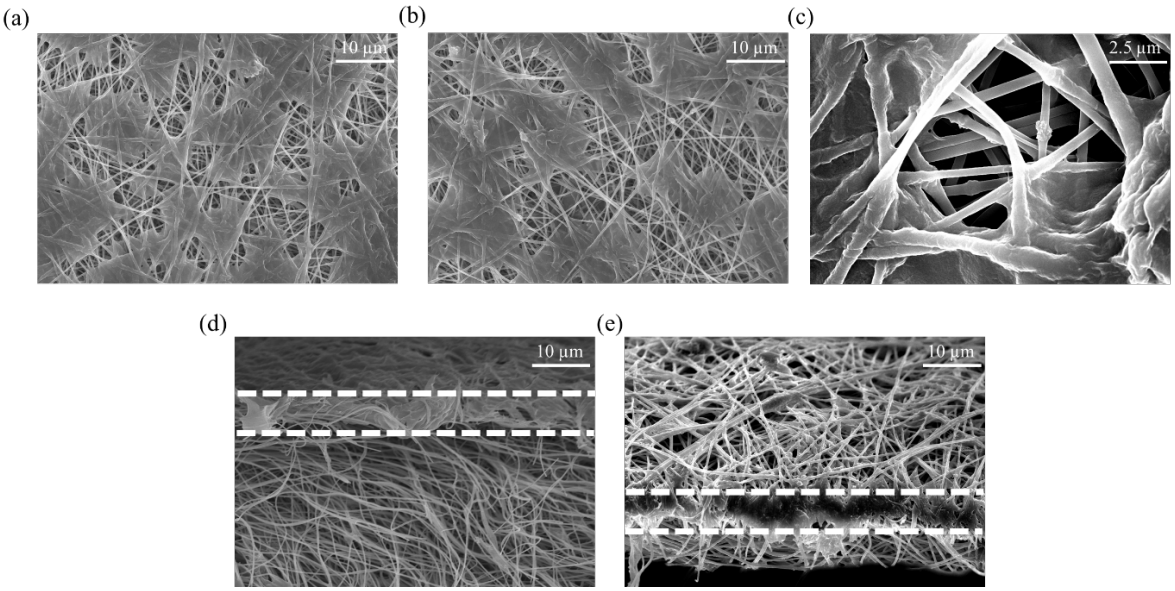

Figure 4. SEM (a-c) surface and (d, e) cross-section images of (a, d) Co-PI-5/5@PE, (b, c, e) Co-PI-5/5-SiO_2@PE.

In Figure S6, both Co-PI-5/5 and Co-PI-5/5-SiO_2 films exhibit perfect affinity to the electrolyte used in LIBs. An increase in only 12° is found after the thin layer of LDPE has been coated onto the above two separators. The contact angles of the above 4 separators are much lower than that of a Celgard2325 separator (52°) due to the low surface polarity of the polyolefin-based separator. These results demonstrate that the LDPE coating does not significantly affect the intrinsic electrolyte affinity characteristics

of PI-based separators.

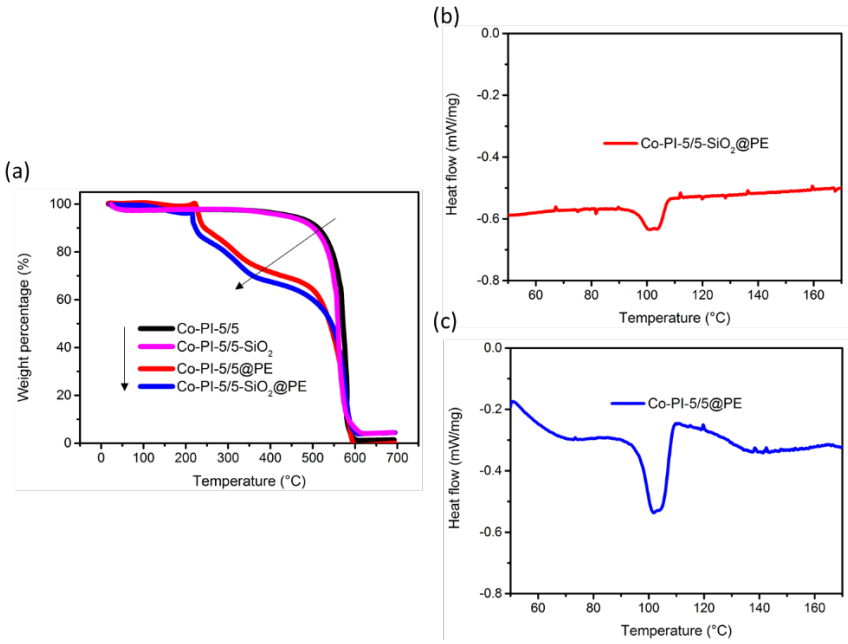

Figure 5. (a) TGA and (b, c) DSC of diagrams of (a1) Co-PI-5/5, (a2) Co-PI-5/5-SiO_2, (a3, b) Co-PI-5/5@PE, and (a4, c) Co-PI-5/5-SiO_2@PE.

TGA and DSC analyses were carried out to examine the thermal properties of LDPE-coated separators and typical results are shown in Figure 5. From Figure 5a, the significant mass loss on the LDPE-coated separators at temperatures between 230 and 500°C is due to the decomposition of LDPE layer. Moreover, Figures 5b and 5c show the endothermic peak at around 100°C, matching the thermal shutdown function test (see Figure S7 in the Supporting Information), which reveals the huge increase in the resistance (from 0.7 to 9000 Ω). The SEM surface and cross-section images of Co-PI-5/5@PE and Co-PI-5/5-SiO_2@PE after the thermal shutdown function test further

confirm the formation of a dense LDPE layer which enables the thermal shutdown function of separators (see Figure S8 in the Supporting Information). On the other hand, the original Co-PI-5/5 film presents the similar TGA responses of polyimide, where the thermal cracking occurs at 500°C and complete decomposition is found at 600°C while the curve for Co-PI-5/5-SiO_2 is similar to that of Co-PI-5/5, except for the 3.5-4.5 % residue after thermal decomposition due to the addition of 5 % SiO_2 NPs.

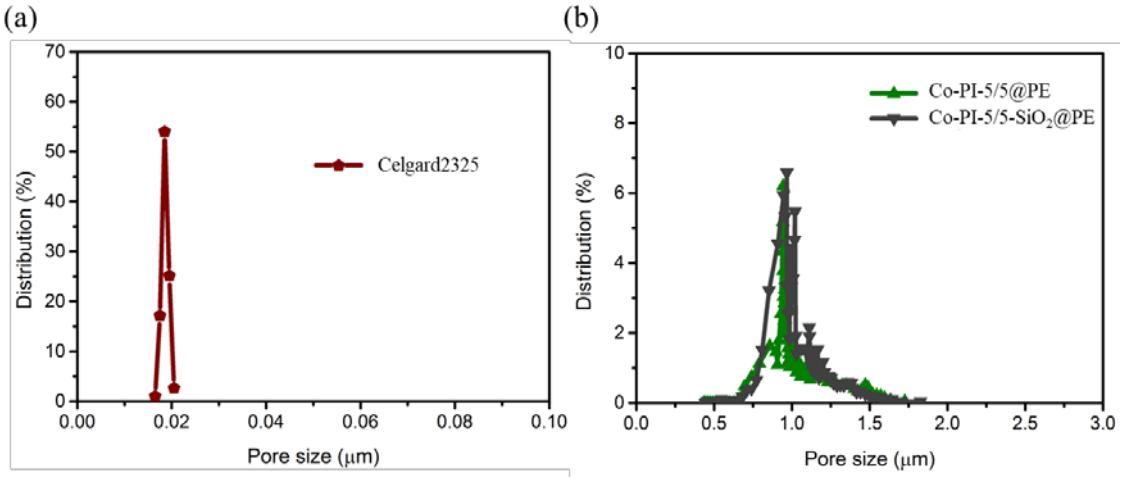

Figure 6. The pore distribution of (a) Celgard2325 and (b) Co-PI-5/5@PE and Co-PI-5/5-SiO_2@PE separators.

The pore size distributions of commercial Celgard2325, Co-PI-5/5-SiO_2@PE and Co-PI-5/5@PE separators are shown in Figure 6. Note that the pore size distribution of the Celgard2325 membrane is narrow, centred at ca. 20 nm. The pore size distributions of the Co-PI-5/5-SiO_2@PE and Co-PI-5/5@PE separators are much broader in comparison with the commercial one. This phenomenon is due to the highly porous nature

of electrospun fabrics although the pore size distribution of these separators becomes narrower after the LDPE coating in comparison with Co-PI-5/5-SiO_2 and Co-PI-5/5 (see Figure S2 in the Supporting Information). The narrowing of pore sizes may prolong the cycle life of LIBs since the charge-discharge currents should be more even and the self-discharge effect is mitigated when the average pore size decreases and the pore size distribution becomes narrower [43].

Table 3. Physicochemical properties of Co-PI-5/5@PE, Co-PI-5/5-SiO_2@PE and Celgard 2325.

Type of separator	Co-PI-5/5@PE	Co-PI-5/5-SiO_2@PE	Celgard2325
Thickness (μm)	25	25	25
Porosity (%)	76	79	43
Electrolyte uptake (%)	1230	1320	98
Ionic conductivity (mS cm^{-1})	1.10	1.40	0.52
MacMullin number	9.5	7.5	20.2

Table 3 compares some physicochemical properties of Co-PI-5/5@PE and Co-PI-5/5-SiO_2@PE separators, including thickness, porosity, electrolyte uptake, and ionic conductivity with the commercially available separator of LIBs (Celgard2325). The capability of electrolyte uptake for both separators developed in this work is much higher than that for Celgard2325 although it slightly decreases with the LDPE coating (see Table 2). Accordingly, the ionic conductivity of Co-PI-5/5-SiO_2 also slightly decreases after this

LDPE layer has been coated onto the separator although the ionic conductivity of Co-PI-5/5-SiO_2 without LDPE is around 4 times of that of Celgard2325 (see Figure S9 for the Nyquist plots of the SS/separator/SS cell in the Supporting Information). Hence, the negative effect of the LDPE coating is minor while an important function, thermal shutdown, has been added on the Co-PI-5/5@PE and Co-PI-5/5-SiO_2@PE separators, meeting one of the essential requirements for the LIBs application.

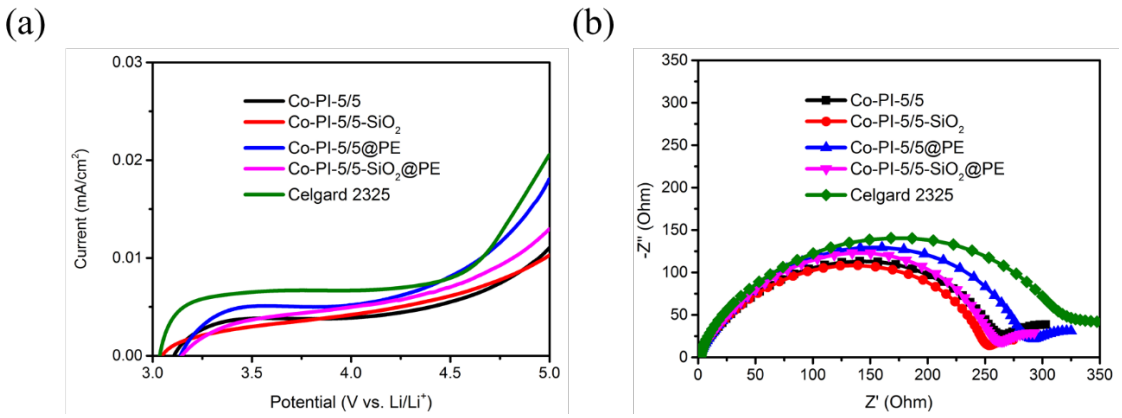

Figure 7. (a) The LSV curves of a Li/separator/SS cell from 3 to 5 V measured at 10 mV s^{-1} and (b) the Nyquist plots of Li/separator/Li cells using (1) Co-PI-5/5, (2) Co-PI-5/5-SiO_2, (3) Co-PI-5/5@PE, and (4) Co-PI-5/5-SiO_2@PE (5) Celgard2325 separators.

Figure 7a show the LSV curves scanned from 3 to 5 V (vs. the Li^+/Li reference electrode) for the Co-PI-5/5, Co-PI-5/5-SiO_2, Co-PI-5/5@PE, and Co-PI-5/5-SiO_2@PE separators. All LSV curves are of very low background currents at potentials more negative than 4.5 V, followed by a slight increment in current flow, probably due to the

reaction(s) among the SS electrode, electrolyte, and separator. Therefore, all of the above separators are compatible with the carbonated-based electrolytes and suitable for the LIB application because of their wide potential windows (> 4.5 V vs. Li^+/Li) for most commercially available positive electrode materials.

The Nyquist plots obtained from the Li/separator/Li cells were employed to determine the charge-transfer responses of Li^+ deposition/stripping and typical results are shown in Figure 7b. The presence of a semicircle on all EIS spectra demonstrates the charge-transfer impedance at the Li/electrolyte interface. From this figure, the order of separators employed in the Li/separator/Li cell with respect to increasing the charge-transfer resistance of Li^+ deposition/stripping is: Co-PI-5/5-SiO_2 (250 Ω) < Co-PI-5/5 (260 Ω) < Co-PI-5/5-SiO_2@PE (270 Ω) < Co-PI-5/5@PE (280 Ω). These results indicate that the compatibility at the Li/separator interface is significantly improved by the addition of SiO_2 into the Co-PI-5/5 nanofibres and that the LDPE layer coated on the PI-based separators increases the charge-transfer resistance of the Li electrode. The former effect favours the electrolyte soaking into the separator to improve the transport of Li ions, reducing charge-transfer resistance of the Li electrode. The latter phenomenon is owning to the decrease in both electrolyte affinity and ionic conductivity when the LDPE layer has been coated on the separators, unfavourable for the redox reactions of Li^+/Li. The charge-transfer resistances are lower than that of the cell containing the Celgard2325

separator (330 Ω), revealing the promising application potential of Co-PI-5/5-SiO_2@PE to the LIBs.

Figure 8(a) shows the results of the first charge-discharge cycle at 0.1 C for the LIBs using a positive $LiFePO_4$ electrode, a negative MCMB electrode, and Celgard2325 or the above 4 separators in a coin-type cell (CR2032) between 2.5 and 4.2 V at room temperature. A comparison of these results indicates that all of the batteries with various separators present stable charge and discharge plateaus with a similar discharge capacity of about 130 mAh g^{-1}, revealing the suitability of all separators for the LIB application. However, the influences of these separators on the cell performance are distinguishable when the discharge current densities are equal to/above 1 C (see Figure 8(b)). For example, the cell employing Co-PI-5/5-SiO_2 shows the smallest voltage difference of the charge and discharge plateaus, owning to the addition of SiO_2, leading to the highest charge-discharge capacity. In addition, the order of separators employed in the cell with decreasing the discharge capacity is: Co-PI-5/5-SiO_2 (93 mAh g^{-1}) > Co-PI-5/5-SiO_2@PE (87 mAh g^{-1}) ≈ Co-PI-5/5 (85 mAh g^{-1}) > Co-PI-5/5@PE (81 mAh g^{-1}) > Celgard2325 (61 mAh g^{-1}). These results are attributable to the improved and declined electrolyte affinity of PI-based separators by the SiO_2 addition and the LDPE coating, respectively, supported by the results in Figure 7. On the other hand, the discharge capacities of all LIBs using the PI-based separators are significantly larger than the one utilizing

Celgard2325, revealing the importance of polymer properties designed for the separators. In fact, the rate capability was tested at the various rates between 0.1 and 2 C and the discharge capacity data of the above cells are presented in Figure 8(c). The variation in discharge capacities are not significant when the rate is below 0.5 C. However, when the charge-discharge rate is equal to/above 1 C, the discharge capacities of the cell using Celgard2325 are much lower than those of the cells using the above four separators, which are about 100 $mAh \cdot g^{-1}$ in 1 C and around 85 $mAh \cdot g^{-1}$ in 2 C. In Figure 8(b), the discharge capacities of the cells using Co-PI-5/5-SiO_2@PE and Co-PI-5/5-SiO_2 are very similar at the 2C rate, indicating that the Co-PI-5/5-SiO_2@PE composite separator shows a minor loss in the charge storage performances but makes the cell safer. In addition, through the introduction of SiO_2 NPs into Co-PI-5/5 nanofibres, the mechanical strength was improved as well as the increased the ionic conductivity of the resultant separators.

The cycling performance of LIBs using the above 5 separators was also tested at 0.5 C for 50 charge-discharge cycles (see Figure 8(d)). Again, the first cycle discharge capacity of the cell is not significantly affected by the separator employed (i.e., Co-PI-5/5 (121 mAh g^{-1}), Co-PI-5/5@PE (120 mAh g^{-1}), Co-PI-5/5-SiO_2 (124 mAh g^{-1}), Co-PI-5/5-SiO_2@PE (122 mAh g^{-1}), and Celgard2325 (118 mAh g^{-1})) because of a relatively low C rate. In addition, the coulombic efficiencies of all cells are close to 100% during the cycling test. The capacity decay rates of all cells are similar in this 50-cycle test while the

capacity retention of the cells using Celgard2325 and Co-PI-5/5-SiO_2@PE is the same considering error variation between cells (89.3% and 88.9%, respectively). In fact, the cells using the PI-based separators coated with a LDPE layer exhibit the capacity retention about 1.2% better than those using the uncoated PI-based films. This minor improvement in the cycle life of LIBs via the LDPE coating is probably attributed to the narrowing of pore sizes and decreasing of the average pore size [43], found in Figure 6. Furthermore, the TEM images of Co-PI-5/5 and Co-PI-5/5-SiO_2 separators before and after the cycling test (see Figure S11 in the Supporting Information) indicate the excellent stability of both separators. In addition, the SiO_2 NPs are still visible on the Co-PI-5/5-SiO_2 separator after the cycling test (also see Figures S12 and S13 in the Supporting Information). On the other hand, it is too difficult to get the TEM images of Co-PI-5/5@PE and Co-PI-5/5-SiO_2@PE because the local heating by electrons melted and burned the LDPE in the TEM.

From all the above results and discussion, a mechanically enhanced, electrospun PI separator with excellent thermal-dimensional stability, good chemical stability, improved electrolyte wettability, and high conductivity has been achieved through the copolymerisation of ODA and PDA with PMDA and the addition of SiO_2 NPs. This separator was found to be suitable for the high-rate energy storage devices, such as the EDLC application. The purpose-oriented function, such as thermal shutdown for the LIB application, can be simply added onto this unique separator by a thin LDPE layer via the

spin coating method (and the spraying method under development). The Li-dendrite inhibition function will be added on this separator in the future in order to further verify the design concept of purpose-oriented functions.

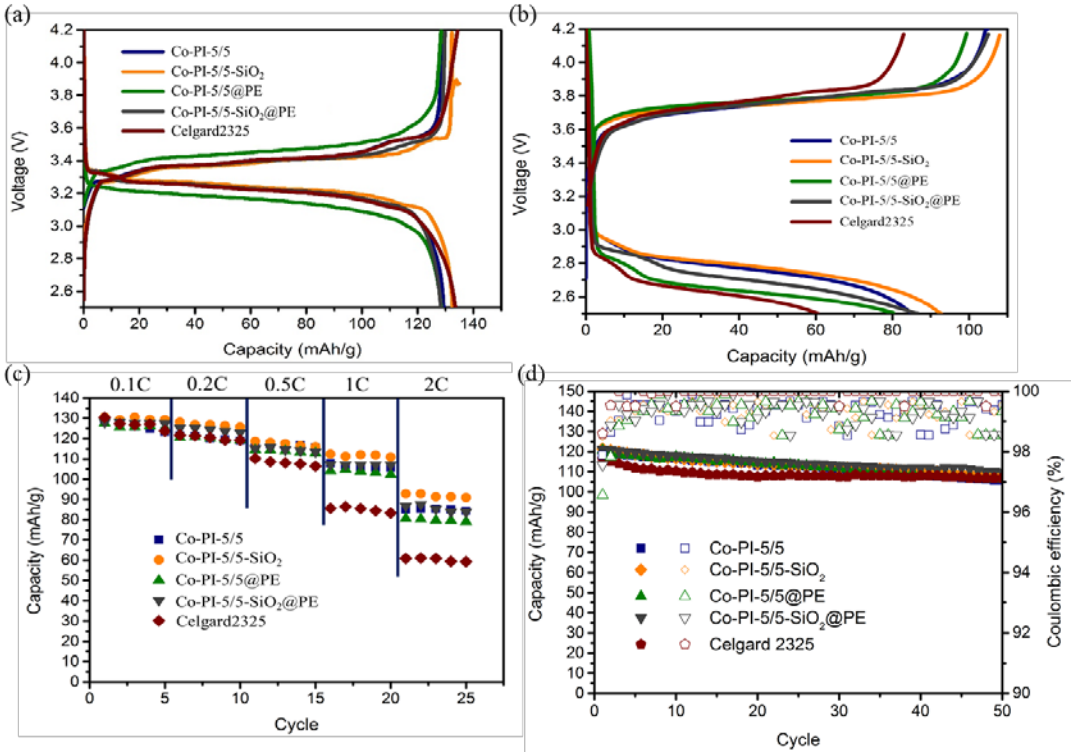

Figure 8. (a) The 1st (0.1 C) and (b) 21st (2 C) charge-discharge cycles, (c) discharge capacity vs. C-rate, and (d) cell capacity vs. cycle number at 0.5 C for the $LiFePO_4$//MCMB cells using (1) Co-PI-5/5, (2) Co-PI-5/5-SiO_2, (3) Co-PI-5/5@PE, (4) Co-PI-5/5-SiO_2@PE, and (5) Celgard2325 separators.

4. Conclusions

The mechanical strength of electrospun PI fabrics can be significantly improved by the copolymerization of 4,4-oxydianiline (ODA) and phenylenediamine (PDA) with pyromellitic dianhydride (PMDA) and the addition of SiO_2 NPs, about triple to the mono PI fabric. The introduction of SiO_2 NPs into copolymerized PI not only enhances the mechanical strength but also promotes the electrolyte uptake and ionic conductivity. The excellent thermo-dimensional stability, good chemical stability, improved electrolyte wettability, and high conductivity of the copolymerized PI-SiO_2 composite separator with controllable thickness is promising for the high-power device applications, such as EDLCs. To further verify the properties of the separators for the LIB application, a thin layer of LDPE was coated on this copolymerized PI-SiO_2 separator in order to provide the thermal shutdown function with an additional benefit on the life cycling because of pore narrowing. This copolymerized PI-SiO_2@PE composite possesses the advantages of high electrolyte uptake and ionic conductivity, highly thermo-dimensional stability, good mechanical strength, high chemical stability, and a thermal shutdown function, demonstrating its great potential as a separator in LIBs. A design concept of purpose-oriented functions for the separators of energy storage devices has been verified in this work.

Acknowledgements

The financial support of this work, by the Ministry of Science and Technology (MOST) of Taiwan under contract no. MOST 106-2923-E-007-005, 107-2923-E-007-001, 108-2923-E-007-001, and National Tsing Hua University under contract no. 109Q2708E1, is gratefully acknowledged.

References

[1] J. Lee, C.-L. Lee, K. Park, I.-D. Kim, J. Power Sources, 248 (2014) 1211-1217.
[2] H. Yu, Q. Tang, J. Wu, Y. Lin, L. Fan, M. Huang, J. Lin, Y. Li, F. Yu, J. Power Sources, 206 (2012) 463-468.
[3] F. Zhang, X. Ma, C. Cao, J. Li, Y. Zhu, J. Power Sources, 251 (2014) 423-431.
[4] K. Tõnurist, T. Thomberg, A. Jänes, I. Kink, E. Lust, Electrochemistry Communications, 22 (2012) 77-80.
[5] C. He, J. Liu, J. Li, F. Zhu, H. Zhao, J. Membr. Sci., 560 (2018) 30-37.
[6] X. Huang, J. Solid State Electrochem., 15 (2011) 649-662.
[7] Y. Xiang, J. Li, J. Lei, D. Liu, Z. Xie, D. Qu, K. Li, T. Deng, H. Tang, ChemSusChem, 9 (2016) 3023-3039.
[8] H. Lee, M. Yanilmaz, O. Toprakci, K. Fu, X. Zhang, Energy & Environmental Science, 7 (2014) 3857-3886.
[9] L. Wang, Z. Wang, Y. Sun, X. Liang, H. Xiang, J. Membr. Sci., 572 (2019) 512-519.
[10] R.S. Borges, A.L.M. Reddy, M.-T.F. Rodrigues, H. Gullapalli, K. Balakrishnan, G.G. Silva, P.M. Ajayan, Scientific reports, 3 (2013) 2572.
[11] A. Jossen, J. Power Sources, 154 (2006) 530-538.
[12] S.S. Zhang, J. Power Sources, 164 (2007) 351-364.
[13] Y. Li, Q. Li, Z. Tan, J. Power Sources, 443 (2019) 227262.
[14] S. Ahn, H. Nara, T. Yokoshima, T. Momma, T. Osaka, Mater. Lett., 245 (2019) 200-203.
[15] Y. Su, G. Chen, L. Chen, Y. Lu, Q. Zhang, Z. Lv, C. Li, L. Li, N. Liu, G. Tan, ACS applied materials & interfaces, 11 (2019) 36697-36704.
[16] R. Mo, F. Li, X. Tan, P. Xu, R. Tao, G. Shen, X. Lu, F. Liu, L. Shen, B. Xu, Nature communications, 10 (2019) 1-10.
[17] L. Liang, X. Sun, J. Zhang, L. Hou, J. Sun, Y. Liu, S. Wang, C. Yuan, Advanced

Energy Materials, 9 (2019) 1802847.
[18] A. Mohammadi Zardkhoshoui, S.S. Hosseiny Davarani, M.M. Ashtiani, M. Sarparast, ACS Sustainable Chemistry & Engineering, 7 (2019) 7908-7917.
[19] A.M. Zardkhoshoui, S.S.H. Davarani, Nanoscale, (2020).
[20] A.M. Zardkhoshoui, S.S.H. Davarani, Chem. Eng. J., 402 (2020) 126241.
[21] A.M. Zardkhoshoui, M.M. Ashtiani, M. Sarparast, S.S.H. Davarani, J. Power Sources, 450 (2020) 227691.
[22] X. Liang, Y. Yang, X. Jin, Z. Huang, F. Kang, J. Membr. Sci., 493 (2015) 1-7.
[23] J. Liu, Y. Liu, W. Yang, Q. Ren, F. Li, Z. Huang, J. Power Sources, 396 (2018) 265-275.
[24] J. Shayapat, O.H. Chung, J.S. Park, Electrochim. Acta, 170 (2015) 110-121.
[25] S. Zheng, L. Wang, X. Feng, X. He, J. Power Sources, 378 (2018) 527-536.
[26] C.-T. Hsieh, S.-C. Lin, C.-H. Lee, C.-F. Liu, C.-C. Hu, J. Electrochem. Soc., 166 (2019) A3132-A3138.
[27] L. Kong, B. Liu, J. Ding, X. Yan, G. Tian, S. Qi, D. Wu, J. Membr. Sci., 549 (2018) 244-250.
[28] A. Haider, S. Haider, I.-K. Kang, Arabian Journal of Chemistry, 11 (2018) 1165-1188.
[29] J.M. Deitzel, J. Kleinmeyer, D. Harris, N.B. Tan, Polymer, 42 (2001) 261-272.
[30] C.-F. Liu, Y.-C. Liu, T.-Y. Yi, C.-C. Hu, Carbon, 145 (2019) 529-548.
[31] Y.-E. Miao, G.-N. Zhu, H. Hou, Y.-Y. Xia, T. Liu, J. Power Sources, 226 (2013) 82-86.
[32] L. Cao, P. An, Z. Xu, J. Huang, J. Electroanal. Chem., 767 (2016) 34-39.
[33] F. Zhang, X. Ma, C. Cao, J. Li, Y. Zhu, J. Power Sources, 251 (2014) 423-431.
[34] H. Cai, X. Tong, K. Chen, Y. Shen, J. Wu, Y. Xiang, Z. Wang, J. Li, Polymers (Basel), 10 (2018).
[35] S. Chen, P. Hu, A. Greiner, C. Cheng, H. Cheng, F. Chen, H. Hou, Nanotechnology, 19 (2008) 015604.
[36] P.-L. Taberna, C. Portet, P. Simon, Appl. Phys. A, 82 (2006) 639-646.
[37] C. Lei, F. Markoulidis, Z. Ashitaka, C. Lekakou, Electrochim. Acta, 92 (2013) 183-187.
[38] A.M. Zardkhoshoui, S.S.H. Davarani, M.M. Ashtiani, M. Sarparast, Journal of Materials Chemistry A, 7 (2019) 10282-10292.
[39] A.M. Zardkhoshoui, S.S.H. Davarani, Nanoscale, 12 (2020) 1643-1656.
[40] A.M. Zardkhoshoui, S.S.H. Davarani, Dalton Transactions, 49 (2020) 10028-10041.
[41] D. He, W. Zhao, P. Li, Z. Liu, H. Wu, L. Liu, K. Han, L. Liu, Q. Wan, F.K. Butt, X. Qu, Appl. Surf. Sci., 465 (2019) 303-312.
[42] H. Peng, G. Ma, K. Sun, Z. Zhang, Q. Yang, Z. Lei, Electrochim. Acta, 190 (2016)

862-871.
[43] P. Arora, Z. Zhang, Chem. Rev., 104 (2004) 4419-4462.